nature geoscience

SUPPLEMENTARY INFORMATION

https://doi.org/10.1038/s41561-019-0485-5

In the format provided by the authors and unedited.

Efficient control of atmospheric sulfate production based on three formation regimes

Jian Xue[1], Xin Yu[1], Zibing Yuan[2], Stephen M. Griffith[3], Alexis K. H. Lau[1,4], John H. Seinfeld[5]* and Jian Zhen Yu[1,3]*

[1]Division of Environment and Sustainability, Hong Kong University of Science and Technology, Kowloon, Hong Kong, China. [2]School of Environment and Energy, South China University of Technology, Guangzhou, China. [3]Department of Chemistry, Hong Kong University of Science and Technology, Kowloon, Hong Kong, China. [4]Department of Civil & Environmental Engineering, Hong Kong University of Science and Technology, Kowloon, Hong Kong, China. [5]Division of Chemistry and Chemical Engineering, California Institute of Technology, Pasadena, CA, USA. *e-mail: seinfeld@caltech.edu; jian.yu@ust.hk

Supplementary Information for

Efficient control of atmospheric sulfate production based on three formation regimes

Jian Xue[1], Xin Yu[1], Zibing Yuan[2], Stephen M. Griffith[3], Alexis K. H. Lau[1,4], John H. Seinfeld[5,*], and Jian Zhen Yu[1,3,*]

[1]Division of Environment & Sustainability, Hong Kong University of Science and Technology, Clear Water Bay, Kowloon, Hong Kong, China.
[2]School of Environment and Energy, South China University of Technology, Guangzhou 510006, China
[3]Department of Chemistry, Hong Kong University of Science and Technology, Clear Water Bay, Kowloon, Hong Kong, China
[4]Department of Civil & Environmental Engineering, Hong Kong University of Science and Technology, Clear Water Bay, Kowloon, Hong Kong, China
[5]Division of Chemistry and Chemical Engineering, California Institute of Technology, Pasadena, CA, 91125, USA

*e-mail: seinfeld@caltech.edu (J.H.S.); jian.yu@ust.hk (J.Z.Y.)

This document contains the following:

Text S1. Comparison of *low-NO_x* and *high-NO_x* regimes defined in the sulfate formation chemical space with those for ozone formation

In this work, the chemical space of sulfate formation is separated into three regimes based on the inflections in the sulfate production isopleths as the NO_x emission rate increases. These three regimes are termed as the *low-NO_x* regime, the *high-NO_x* regime and the *NO_2-oxidant* regime to reflect the key characteristic or role of NO_x or NO_2 in each regime. The terms for the first two regimes are also used to describe ozone formation chemical regimes[1-2],

The *low-NO_x* and the *high-NO_x* regimes identified in the sulfate formation chemical space do not equate to those in the O_3 production regimes. However, we note there are similarities. In both paradigms, the target secondary pollutant (O_3 or sulfate) is driven by increased NO_x in the *low-NO_x* regime and limited by NO_x in the *high-NO_x* regime.

In the haze-fog scenarios that are interpreted in this study, the aqueous phase reaction of O_3 and $S_{(IV)}$ is the dominant pathway for sulfate formation in the *low-NO_x* and *high-NO_x* regimes (Regimes 1 and 2) (Figure S3). Therefore, the distinction between *low-NO_x* and *high-NO_x* is at least qualitatively related to the NO_x-limited / NO_x saturated regime splitting for ozone simulation (see Figure ST1 below). Figure ST1 shows the simulated ozone isopleths as a function of NO_x and SO_2 emission rates under haze-fog conditions considered in this study.

Below, we analyze the boundary values of NO_x that separate the different regimes in the two paradigms for ozone and sulfate. As described by Wennberg[1], the level at which to draw the line between *low-* and *high-NO_x* for ozone production is dependent on other factors (e.g., VOC concentration). Similarly, as shown in Figure 2 here, the boundary between *low-* and *high-NO_x* for sulfate production is also dependent on an array of other factors (e.g., VOCs, pH of atmospheric aqueous phase). Wennberg states "Within the air quality community, high-NO_x is often used to describe environments that are NO_x-saturated with respect to production of oxidants, in particular ozone (O_3). In such environments where NO_x concentrations are measured in 10s of ppb or more, the production rate of O_3 is either independent of or decreases with additional NO_x." Sillman[2] states "NO_x-saturated chemistry occurs at lower NO_x concentrations in the remote troposphere than in polluted regions (1 ppb or higher in the remote troposphere, 5-10 ppb or higher in polluted regions) because the radical source (driven by lower H_2O in reaction (R7)) is lower.

$$O_3 + h\nu \xrightarrow{H2O} 2OH \text{ (R7 in ref. 1)}$$

The NO_2 concentration value at the boundary between the *low-NO_x* and *high-NO_x* regimes in the sulfate formation chemical space shown in Figure 2 ranges from ~4-15 ppb.

Figure ST2 shows the model-predicted diurnal concentrations of NO, NO_2 and O_3 at typical NO_x and SO_2 emission rates that lay on the transfer line separating the *Low-NO_x* and *High-NO_x* regimes in Figure 2 (Emission: SO_2=1 ppb h^{-1}, NO_x=0.4 ppb h^{-1}, HC = 4 ppb h^{-1}, CO=2 ppb h^{-1}). NO_2 dominates the afternoon NO_x concentration when the majority of O_3 is produced. The overall NO_x concentration ranges from a few ppb to ~25 ppb, close to the range of "10s of ppb NO_x" estimated by Wennberg[2] and within the "5-10 ppb in polluted regions" estimated by Sillman[2]. Meanwhile, the concentration of NO was between 200-400 ppt, well below the level under which NO dominates peroxy radical chemistry (IGAC news 2013, Quote: "Such NO dominant peroxy radical chemistry occurs in the atmosphere (and many laboratory studies) when NO concentrations are typically greater than 2×10^{10} molecules cm^{-3} (>~1 ppb at 1 atm)".

In summary, the *low-NO_x* and *high-NO_x* splitting in the sulfate formation regimes do not equate to but are qualitatively related to the NO_x-limited / NO_x saturated regime splitting for ozone formation in the scenarios simulated in this work.

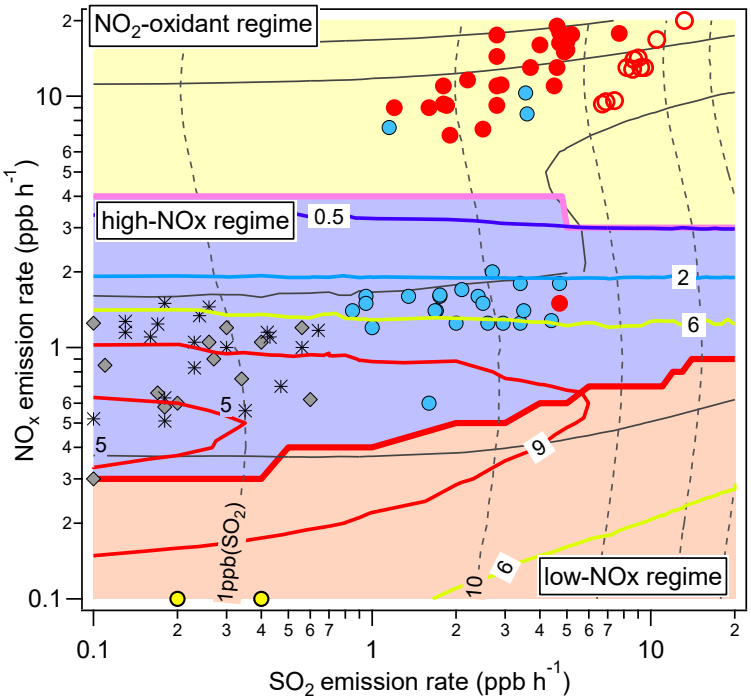

Figure ST1 Simulated daily averaged O_3 concentration (ppb) as a function of NO_x and SO_2 emission rates under haze-fog conditions**.** This simulation was conducted at an aqueous phase pH of 5.6. The colored curves show isopleths of daily averaged O_3 concentration (ppb), with the colder colors representing lower concentration and warmer colors representing higher concentration. Isopleths of the daily averaged NO_2 concentration are given by solid curves. Isopleths of the daily average SO_2 concentration are given by dashed curves. Solid red and pink lines delineate three individual SO_4^{2-} formation regimes.

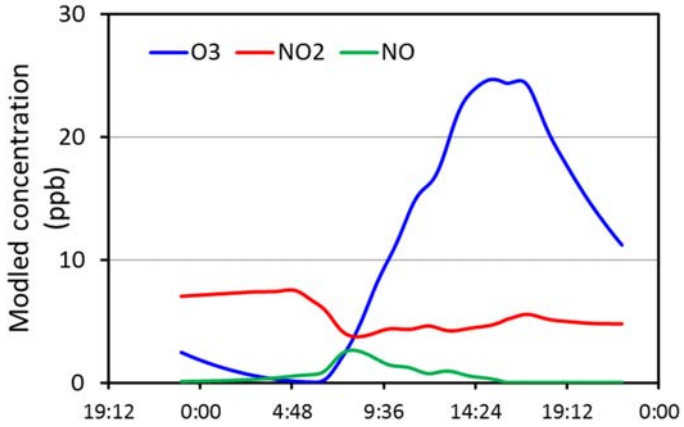

Figure ST2. Diurnal NO, NO_2 and O_3 concentration predicted under a typical condition on the transfer line between Low-NO_x and High-NO_x regimes in Figure 2 (Emission: SO_2=1 ppb h^{-1}, NO_x=0.4 ppb h^{-1}, HC = 4 ppb h^{-1}, CO=2 ppb h^{-1}).

Text S2 Calculation of sulfate formation contributed by the $S_{(IV)}$+NO_2 pathway during haze episodes in northern China

If mass transfer limitations are not taken into account, sulfate formation contributed by the pathway of $S_{(IV)}$+NO_2 can be estimated as,

$$\frac{dSO_4^{2-}}{dt} = k_{(NO2)}[S_{(IV)}][NO_2(aq)]$$
$$= k_{(NO2)}H(T)_{(SO2)}p_{(SO2)}[1 + \frac{K(T)_{S1}}{[H^+]} + \frac{K(T)_{s1}K(T)_{s2}}{[H^+]^2}]H(T)_{(NO2)}p_{(NO2)}$$

where,

$$H(T)_{(SO2)} = H(298K)_{(SO2)}\exp\left(\frac{\Delta H_{(SO2)}}{R}\left(\frac{1}{298} - \frac{1}{T}\right)\right)$$
$$H(T)_{(NO2)} = H(298K)_{(NO2)}\exp\left(\frac{\Delta H_{(NO2)}}{R}\left(\frac{1}{298} - \frac{1}{T}\right)\right)$$
$$K(T)_{s1} = K(298K)_{s1}\exp\left(\frac{\Delta H_{S1}}{R}\left(\frac{1}{298} - \frac{1}{T}\right)\right)$$
$$K(T)_{s2} = K(298K)_{s2}\exp\left(\frac{\Delta H_{S2}}{R}\left(\frac{1}{298} - \frac{1}{T}\right)\right)$$

Here, T=271 K is the typical ambient temperature during the haze episode; pH was set to be 5.8 the average for aerosol liquid estimated by Cheng et al.[3]; $H(298\ K)_{(SO2)}$=1.23 M atm^{-1}, $H(298\ K)_{(NO2)}$=0.01 M atm^{-1}, $K(298\ K)_{(S1)}$=0.013 M, $K(298\ K)_{(S2)}$=6.6×10^{-8} M are the Henry's constants for SO_2, the Henry's constants for NO_2, dissociation constant for H_2SO_3 and dissociation constant for HSO_3^- at 298 K, respectively; $\Delta H_{(SO2)}$=−6250 cal mol^{-1}, $\Delta H_{(NO2)}$=−5000 cal mol^{-1}, $\Delta K_{(S1)}$= −3893 cal mol^{-1}, $\Delta K_{(S2)}$= −2979 cal mol^{-1} are the corresponding heats of dissolution for Henry's law constant at 298 K; $p_{(SO2)}$ =40 ppb and $p_{(NO2)}$ = 66 ppb are the typical ambient SO_2 and NO_2 concentrations given by Cheng et al..[3]; $k_{(NO2)}$=2×10^6 M^{-1} s^{-1}, is the reaction rate of $S_{(IV)}$+NO_2. The sulfate formation rate contributed by the pathway of $S_{(IV)}$+NO_2 is maximally 0.7 μg m^{-3} h^{-1}. If a higher reaction rate $k_{(NO2)}$=1.3×10^7 M^{-1} s^{-1} is taken[1], this value could reach 4.6 μg m^{-3} h^{-1}.

Text S3 Impact of under-estimated OH radical concentration on sulfate formation during haze/fog episode conditions

Figure S11 shows the diurnal variation of OH and H_2O_2 predicted by a previously developed observation-based model for secondary inorganic aerosols (OBM-SIA). OH radical concentrations are predicted to have peaked at 2 pm with maximum concentrations ranging from 2.5-8.9×10^5 molecules cm^{-3}. Noontime OH radical concentrations of 2.4×10^6 molecules cm^{-3} on average were measured during several severe air pollution events in Beijing[4]. Our predicted noontime OH concentration is up to one order of magnitude lower than this measured OH level.

Based on the observation of OH radicals, Tan et al.[4] estimated that the daytime averaged SO_2 oxidation rate through the reaction of OH+SO_2 was 0.02 ppbv h^{-1} (=0.09 μg m^{-3} h^{-1} at 0ºC 1atm), far lower than the sulfate production rates required to explain observations during the haze episodes (~3 μg m^{-3} h^{-1}, Cheng et al.[3]) and haze-fog episodes (up to 9.6 μg m^{-3} h^{-1}, this study).

If we assume, during a typical winter episode in north China, noontime OH and HO_2 concentrations of 2.4×10^6 and 1×10^8 molecules cm^{-3}, respectively[4], and each H_2O_2 produced through Reaction (1) yields sulfate through Reaction (3), the sulfate formation rates through Reactions (1) & (2) are estimated to be ~0.9 μg m^{-3} h^{-1} at noon time and ~0.2 μg m^{-3} h^{-1} on average for the day (when SO_2=25 ppb), close to the estimation by Tan et al. [4] Thus, the elevated HO_x levels measured in Tan et al cannot explain the fast formation of sulfate interpreted in this study.

$$HO_2 + HO_2 \rightarrow H_2O_2 + O_2 \quad \text{(Reaction 1)}$$

$$OH + SO_2 \rightarrow HO_2 + sulfate \quad \text{(Reaction 2)}$$

$$H_2O_2(aq.) + HSO_3^-(aq.) + H^+ \rightarrow sulfate + 2H^+ + H_2O \quad \text{(Reaction 3)}$$

Table S1 Value, location and references of the paired SO_2/NO_2 data presented in Figure 1

Category	Location	Year	SO_2[#]	NO_2[#]	Reference
Rural U.S.	Pennsylvania	2016	1.34	1.22	5
	California		0.04	0.30	
	California		0.00	0.79	
	California		0.56	1.19	
	California		0.05	1.76	
	California		0.06	0.61	
	California		0.64	0.44	
	California		0.17	0.75	
	California		0.77	1.21	
Rural PRD, China	Tianhu, Guangzhou	2015	3.76	4.70	6
	TaMen, HongKong		3.01	5.75	
Urban US, 2015	California	2015	0.76	13.98	5
	California		0.99	19.78	
	California		0.17	22.23	
	California		0.51	10.47	
	California		0.30	12.81	
	New York		1.83	20.13	
	New York		1.29	17.10	
	New York		1.04	11.10	
	New York		0.75	17.16	
	Pennsylvania		1.80	8.54	
	Pennsylvania		0.58	9.01	
	Florida		0.04	4.09	
	Virginia		0.47	8.18	
	Michigan		0.87	6.94	
Urban Europe, 2015	Paris centre	2015	0.37	22.41	7, 8
	London centre		0.76	23.33	
	Milan		0.86	24.63	
	Roma		0.62	25.83	
	Lyon		0.43	18.93	
	Munich		1.80	16.17	
	Luxembourg		1.36	17.56	
	Brussels		1.36	19.08	
	Birmingham		0.45	18.48	
	Amsterdam		0.50	20.85	
	Bremen		0.67	12.87	
	Praha		0.65	16.72	
	Poznan		1.35	10.04	
	Istres		0.51	6.92	
	Lorient		0.14	7.14	
	Dublin		0.91	16.13	
	Mores		0.47	8.66	
	Madrid		2.08	19.04	
	Cognac		0.99	7.66	
Megacities, China, 2010-2015	Luhu, Guangzhou	2015	3.38	25.61	6
	liyuan, Shenzhen		3.38	20.38	
	Jinjuzhe, Foshan		6.39	23.52	
	Huijingcheng, Foshan		7.14	28.22	
	Quanwan, HongKong		5.63	33.45	
	Yuanlang, Hong Kong		3.38	25.09	
	Dongchong, Hong Kong		3.01	22.47	
	DongHu, Jiangmen		6.01	19.34	
	Wanqingsha, Guangzhou	2010	12.99	24.98	9
	Luhu, Guangzhou		10.70	27.64	
	Jinjuju, Foshan		16.43	28.17	
	Huijingcheng, Foshan		18.34	36.68	
	Haogang, Dongguan		12.61	27.64	

	Xiapu,Huizhou		6.11	19.14	
	Jinguowan, Huizhou		5.35	10.10	
	Zimang, Park, Zhongshan		9.17	21.26	
	Chengzhong, Zhaoqing		17.96	30.83	
	Donghu, Jiangmen		13.37	17.54	
	Beijing		12.23	30.35	10
Megacities, China, 2010-2015	Shanghai		10.70	26.53	11
	Beijing	2015	5.03	26.13	12
	Shanghai,PuTuo		6.39	24.04	13
	Jinan		18.78	25.09	14
	Nanjing	2014	9.39	28.22	15
	Hangzhou		7.89	26.13	16
	Chengdu		5.26	27.70	17
	Nanjing	2006-2007	57.06	59.54	18
	Nanjing		57.06	54.58	
	Nanjing		71.32	69.46	
	Nanjing		46.36	44.65	
	Nanjing		39.23	29.77	
	Nanjing		49.93	39.69	
Haze-fog megacities, China	Nanjing		46.36	39.69	
	Nanjing		35.66	29.77	
	Nanjing		35.66	29.77	
	Guangzhou	2005	43.89	57.45	19
	Guangzhou		48.76	41.28	
	Guangzhou		48.30	45.06	
	Hong Kong	2009	22.90	80.66	20
	Shanghai,	2013	14.27	58.27	21
	Shanghai,	2014-2015	26.29	71.08	
	Shanghai		24.42	62.71	
	Beijing		26.29	57.49	22,23*
	Beijing		25.35	54.87	
	Beijing		23.66	52.26	
	Beijing		40.00	66.00	
	Guangzhou		13.90	75.78	
	Beijing		25.35	62.71	
	Beijing		23.29	39.20	
	Beijing		22.54	47.04	
	Beijing		17.65	20.90	
Haze megacities, China	Beijing		13.90	41.81	
	Beijing		9.39	36.58	
	Beijing		11.27	47.04	
	Shanghai		24.42	71.60	
	Shanghai		19.16	49.13	
	Shanghai		5.63	36.58	
	Shanghai		20.28	62.71	
	Shanghai		13.90	41.81	
	Shanghai		8.64	36.58	
	Guangzhou		9.02	42.85	
	Guangzhou		12.40	31.36	
	Guangzhou		7.89	36.06	
	Guangzhou		13.52	35.01	
	Guangzhou		9.39	31.36	
Haze, megacities, India	Delhi	2007-2008	14.01	22.47	24
	Delhi		2.70	29.27	
WHO, annual standard		2005	7.51	20.90	25

#: Data in μg m^{-3} were converted to ppb assuming at 20°C 1 atm.

*:Read from the figures.

Table S2 Emission rates and other parameters

Scenario/parameters	Guangzhou fog-haze (winter, megacity China)	Typical fog (summer, rural eastern U.S.)
Meteorological parameters		
Solar insolation	Calculated based on observation of ground level solar radiation rate during haze episodes in GZ	100% cloud coverage summer value [26] Central Pennsylvania, U.S.
Mixing layer height(m)	300-450	300-450
Temperature(°C)	17-20	16-30
Humidity (%)	100	100
Emissions		
HC (ppb h^{-1})*	4	0.4
CO (ppb h^{-1})	2	0.2
SO_2 (ppb h^{-1})	0.1-20	
NO_2 (ppb h^{-1})	0.1-20	
NO_2/NO_x	0.053	0.053
Fog/cloud		
pH	5.6	4.7 [26]
Droplet radius (μm)	5	5
Water content (mg m^{-3})	40	40
Mn(II) (μg/L)	534	2.2 [26,#]
Fe(III) (μg/L)	336	17.2 [26,#]
Aerosol		
Surface area density (m^{-2} m^{-3})	2.21×10^{-3}	1.00×10^{-4}
Uptake coefficient of SO_2	5×10^{-4}	5×10^{-4}

*: Emission rates for individual HC species are listed in Table S3.
#: Assume half of the measured soluble Mn and Fe are Mn(II) and Fe(III), respectively.

Table S3 Emission rates of individual hydrocarbon species based on carbon atom ratio

Species	HC Emission based on carbon atom (%)*
HCHO	0.8
Acetaldehyle	1
Formic acid	0.07
Acetic acid	0.14
Ethane	4.7
Propane	10.1
Higher alkane	40.4
Ethylene	6.4
Higher alkene	11.3
Toluene#	12.55
Xylene*	12.55

* Follows Table 3 in Kleinman (1991)[27].
# We use toluene and xylene to represent aromatic compounds.

Table S4 Chemical species and their initial concentrations

Seq.	Gas	Initial C(ppb)	Seq.	Gas	Initial C(ppb)		Gas	Initial C(ppb)
1	NO	1	31	ETHA	0	61	CTERP	0
2	NO_2	1	32	ROOH	0			
3	O_3	0	33	AACD	0			
4	O	0	34	PACD	0	**Seq.**	**Aqueous**	**Initial C(μM)**
5	$O(^1D)$	0	35	PAR	5	1	O_2	0
6	OH	$2*10^{-13}$	36	ROR	0	2	O_3	0
7	HO_2	$2*10^{-12}$	37	ETH	0	3	H^+	
8	H_2O_2	0	38	OLE	0	4	NO_2aq	0
9	NO_3	0	39	IOLE	0	5	H_2O_2	0
10	N_2O_5	0	40	ISOP	0.17	6	$SO_2.H_2O$	0
11	HONO	0	41	ISPD	0	7	HSO_3^-	0
12	HNO_3	0	42	TERP	0	8	SO_3^{2-}	0
13	PNA^b	0	43	TOL	0	9	NO_2^-	0
14	CO	200	44	XYL	0	10	NO_3^-	0
15	FORM	0	45	CRES	0	11	Sulfaq	0
16	ALD_2	0	46	TO_2	0	12	OHaq(radi)	0
17	C_2O_3	0	47	OPEN	0	13	SO_3^-(radi)	0
18	PAN	0	48	CRO	0	14	SO_5^-(radi)	0
19	ALD_X	0	49	MGLY	0	15	HSO_5^-	0
20	C_XO_3	0	50	SO_2	1/0.1*	16	SO_4^-(radi)	0
21	PAN_X	0	51	H_2O	2.5%	17	$S_2O_6^{2-}$	0
22	XO_2	0	52	H_2	550	18	$S_2O_8^{2-}$	0
23	XO_2N	0	53	HCO_3	0	19	HCHOaq	0
24	NTR	0	54	O_2	21%	20	HMS	0
25	ETOH	0	55	CETH	0	21	$H_2C(OH)_2$	0
26	CH_4	1700	56	COLE	0	22	HO_2aq(radi)	0
27	MEO_2	0	57	CIOLE	0	23	O_2^-	0
28	MEOH	0	58	COPEN	0	24	HO_2(radi)	0
29	MEPX	0	59	CISOP	0	25	Fe(III)	6
30	FACD	0	60	CISPD	0	26	Mn(II)	9.7

*: Initial SO_2 was set to be 1 ppb for simulation in Guangzhou and 0.1 ppb for simulation in rural US.

Table S5 Full names of abbreviated species in Table S3

Species	Name Description	Number of Carbons	Molecular Weight
PNA	Peroxynitric acid (HNO_4)	0	79
FORM	Formaldehyde	1	30
ALD2	Acetaldehyde	2	44
C2O3	Acetylperoxy radical	2	75
PAN	Peroxyacetyl nitrate	2	121
ALDX	Propionaldehyde and higher aldehydes	2	44
CXO3	C3 and higher acylperoxy radicals	2	75
PANX	C3 and higher peroxyacyl nitrates	2	121
XO2	NO to NO2 conversion from alkylperoxy (RO2) radical	0	1
XO2N	NO to organic nitrate conversion from alkylperoxy (RO2) radical	0	1
NTR	Organic nitrate (RNO3)	1	130
ETOH	Ethanol	2	46
MEO2	Methylperoxy radical	1	47
MEOH	Methanol	1	32
MEPX	Methylhydroperoxide	1	48
FACD	Formic acid	1	46
ETHA	Ethane	2	30
ROOH	Higher organic peroxide	1	62
AACD	Acetic and higher carboxylic acids	2	60
PACD	Peroxyacetic and higher peroxycarboxylic acids	2	46
PAR	Paraffin carbon bond (C-C)	1	14
ROR	Secondary alkoxy radical	0	31
ETH	Ethene	2	28
OLE	Terminal olefin carbon bond (R-C=C)	2	27
IOLE	Internal olefin carbon bond (R-C=C-R)	4	48
ISOP	Isoprene	5	68
ISPD	Isoprene product (lumped methacrolein, methyl vinyl ketone, etc.)	4	70
TERP	Terpene	10	136
TOL	Toluene and other monoalkyl aromatics	7	92
XYL	Xylene and other polyalkyl aromatics	8	106
CRES	Cresol and higher molecular weight phenols	8	108
TO2	Toluene-hydroxyl radical adduct	7	109
OPEN	Aromatic ring opening product	4	84
CRO	Methylphenoxy radical	7	139
MGLY	Methylglyoxal and other aromatic products	3	72
NO_2E	electronically excited NO_2	0	46

Table S6 Simplified aqueous phase reactions for sulfate formation

Seq.	Reactions	Reaction constant at 298K(M^{-1} s^{-1})	E/R(K)	Ref.(1)
R1	$OH + HO_2 \rightarrow H_2O + O_2$	7.0E+09	1500	28
R2	$O_3 + O_2^- \rightarrow OH + 2O_2 + OH^-$	1.5E+09	1500	28
R3	$OH + O_2^- \rightarrow O_2 + OH^-$	1.0E+10	1500	28
R4	$HO_2 + HO_2 \rightarrow H_2O_2 + O_2$	8.6E+05	2365	28
R5	$OH + H_2O_2 \rightarrow H_2O + HO_2$	2.7E+07	1700	28
R6	$HO_2 + O_2^- \rightarrow H_2O_2 + O_2 + 2OH^-$	1.0E+08	1500	28
R7	$OH + O_3 \rightarrow HO_2 + O_2$	2.0E+09		28
R8	$HO_2 + O_3 \rightarrow OH + 2O_2$	1.0E+04		28
R9	$OH + SO_3^{2-} \rightarrow H_2O + SO_3^-$(radi)	450E+09		28
R10	$OH + HSO_3^- \rightarrow H_2O + SO_3^-$(radi)	5.20E+09		28
R11	SO_3^-(radi) + O_2(aq) → SO_5^-(radi)	1.50E+09		28
R12	SO_5^-(radi) + HSO_3^- → HSO_5^- + SO_3^-(radi)	2.50E+04	3100	28
R13	SO_5^- (radi) + SO_3^{2-} → HSO_5^- + SO_3^-(radi)	2.50E+04	2000	28
R14	SO_5^-(radi) + HSO_3^- → SO_4^-(radi) + sulfate	7.50E+04		28
R15	SO_5^-(radi) + SO_3^{2-} → SO_4^-(radi) + sulfate	7.50E+04		28
R16	SO_4^-(radi) + HSO_3^- → sulf ate+ SO_3^-(radi)	7.50E+08		28
R17	SO_4^-(radi) + SO_3^{2-} → sulfate + SO_3^-(radi)	5.50E+08		28
R18	SO_5^-(radi) + SO_5^-(radi) → 2*SO_4^-(radi)	6.00E+08	1500	28
R19	SO_3^-(radi) + SO_3^-(radi) → $S_2O_6^{2-}$	7.00E+08		28
R20	SO_4^-(radi) + SO_4^-(radi) → $S_2O_8^{2-}$	4.50E+08		28
R21	SO_5^-(radi) + SO_5^-(radi) → $S_2O_8^{2-}$-	1.40E+08		28
R22	HSO_5^- + HSO_3^- +H^+→ 2*sulfate+3H^+	7.10E+06		28
R23	$O_3 + SO_2 \bullet H_2O$ → sulfate+O_2	2.4E+04		28
R24	O_3 + HSO_3^- → sulfate+O_2	3.7E+05	5530	28
R25	O_3 + SO_3^{2-} → sulfate+O_2	1.5E+09	5280	28
R26	(O_2) + $S_{(IV)}$ (Fe(III)) → sulfate+O_2	*p*H=5.6, R=1.E-03/15[S(IV)](2) *p*H=4.7, R=1.2E+06[Fe(III)][SO_3^{2-}]		28
R27	(O_2) + $S_{(IV)}$ (Mn(II)) → sulfate+O_2	R=680*$10^{-4.07\alpha/(1+\alpha)}$ [Mn(II)]^2 (3) (S(IV)>1 μM) R=1.0E+03[Mn(II)][S(IV)] (S(IV)<1 μM)		28
R28	$2NO_2 + HSO_3^-$→ 3H^++sulfate+2NO_2^-	*p*H=4.7,k=1.4E+05 (4) *p*H=5.6, k=2.0E+06		28
R29	HCHO + HSO_3^- → HMS	7.9E+02	4900	28
R30	HCHO + SO_3^{2-} → HMS+ OH^-	2.5E+07	1800	28
R31	HMS+ OH^- → HCHO + SO_3^{2-} + H_2O	3.6E+03	4500	28
R32	HMS+ OH → HCHO + SO_5^-(radi) + H_2O	2.6E+08	1500	28
R33	NO+ NO_2 →2NO_2^-+ 2H^+	2.E+08	1500	28
R34	NO_2 + NO_2 →NO_2^-+ NO_3^- + 2H^+	1.E+08	1500	28

(1) Seinfeld and Pandis (2006) and references therein, p306-336[28];
(2) The rate constant is divided by 15 for the simulation of haze-fog because "near urban areas formate could reduce the rate of the catalyzed oxidation by a factor of 10-20 in the high-pH regime." (Martin et al.[29] (see Seinfeld and Pandis, p315 and appendix 4 in the document) [28];
(3) $\alpha=(I)^{0.5}$, where I is the ionic strength, calculated using the ionic composition observed during haze-fog events in Nanjing[18]. Martin and Hill (1987)[30] suggested the zero-order kinetics was applicable for $S_{(IV)}$ above 100 μM. Here we extended it down to 1 μM because the reaction rate in $S_{(IV)}$ concentration range between 1 and 100 μM is not well constrained.
(4): According to Lee and Schwartz (1983)[31] and Seinfeld and Pandis (2006)[28], the reaction can be described as $k[(S_{(IV)})[NO_2]$. The reaction rate k is pH-dependent. At pH=5.0, $k=1.4\times10^5$, while at pH=5.8 and 6.4, only a lower limit, $k=2.0\times10^6$, can be determined. In this study, k was approximated as 1.4×10^5 at pH=4.7, and 2.0×10^6 at pH=5.6. Part of this table has been presented in the supporting information in our previous work[32].

Table S7 Dry deposition velocities (V_{gi}, cm s^{-1}) adopted in the model

Species	V_{gi} (cm s^{-1})
CO	0.03
NO	0.016
NO2	0.1
HNO3, FACD, AACD	4
O3	0.4
H_2O_2	0.5
SO2	0.5
HONO	0.5
FORM, ALD2,ALDx	0.25
Others	0

Table S8 Gas-phase diffusion coefficients (D_{gi}, cm^2s^{-1}) adopted in the model

Species	D_{gi}
N_2O_5	0.09
NO_2	0.14
NO_3	0.12
O_3	0.12
OH	0.23
SO_2	0.12
Others	0.10

Table S9 Mass accommodation coefficients (α_{gi}) adopted in the model

Species	α_{gi}
O_2	0.01
O_3	0.004
OH	0.004
HO_2	0.01
H_2O_2	0.11
HCHO	0.01
FACD	0.013
NO	0.02
NO_2	0.001
N_2O_5	0.02
HNO_2	0.05
HNO_3	0.05
SO_2	0.1
NH_3	0.09
others	Not applied

Table S10. Parameters of the fog events documented in downtown Chinese megacities and in the U.S.

Location	Formation date	Duration (h)	Fog water pH	SO_4^{2-} (μeq/L)	NH_4^+ (μeq/L)	Ca^{2+} (μeq/L)	Ca^{2+}/NH_4^+	Ref.
Nanjing, China.9 events	11/12/2006	18.5	5.9 ±1.0	6969 ±6506	6654 ±6750	3772 ±3458	0.57	18
	13/12/2006	13.8						
	24/12/2006	67.5						
	13/12/2007	13.5						
	18/12/2007	8.7						
	18/12/2007	20.4						
	19/12/2007	23.6						
	20/12/2007	25.3						
	22/12/2007	7.3						
Guangzhou, China. 3 events	25/02/2005	24	5.35	70842	20048	11168	0.56	19
	15/03/2005	60	5.75	51130	9870	53726	5.44	
	29/03/2005	36	5.85	2395	718	3450	4.80	
Shanghai, China,26 events	2009-10	0.5-24	5.97 (4.68-6.58)	2830	4005	2064	0.52	33
Central Pennsylvania U.S.	2007-2010		4.74 (3.08-7.41)	140.8	260	77.1	0.30	34
SJV, California U.S.	Winter 00/01		6.73 (5.85-8.04)	56.5	608.3	10.7	0.02	35
Louisiana U.S.	Winter 04/05		5.0 (2.76-6.37)	1791.4	2077.8	29.9	0.01	36
Houston, U.S.	Winter 2006		4.3 (3.19-7.19)	952.9	865.5	251.5	0.29	36

Table S11 Studies reporting observations of haze events characteristic of high NO_x and high sulfate

Seq*	Study^	Observation Time	Location	RH	SO_2# (ppb)	NO_x# (ppb)	Sulfate# ($\mu g/m^3$)
HZ1	Han et al, 2015	Aug-Sep 2006	Beijing	20-100%	up to ~40	up to ~80	50
HZ2	Kong et al, 2018	18-28 Feb. 2011	shanghai	45-90%	10-22	15-30	13-18
HZ3	Xie et al, 2015	Apr-Jun 2012	Nanjing	60-90%	5-25	20-80	20-80
HZ4	Zhao et al, 2016	Nov 2013-Jan 2014	Shanghai	30-90%	22.00	46.00	21.50
HZ5	He et al, 2014	Jan 2013	Beijing urban	_ϕ	19 (mean) up to 60	100 (mean) up to 250	up to 155
HZ6	Huang et al, 2019	5-7 Dec. 2013	Yangtze River Delta	56% (~20-100%)	24	91	36
HZ7	Wang et al, 2016	Jan 2013	Yangtze River Delta	55-90%	18 (14-25)	41 (38-50)	–
HZ8	Gao et al, 2016	25-30 Jan 2013	North China	20-100%	25-80	25-125	60 (mean) up to ~150
HZ9	Liu et al, 2016	2014 haze days	Beijing & Baoding	20-75%	up to 80	up to 100	22-36
HZ10	He et al, 2018	Oct 2014-Jan2015	Beijing	35-80%	_	_	28.4 (8.2-56)
HZ11	Chen et al, 2016	Oct 2014 (4 episodes)	Beijing	20-100%	5-30	20-140	up to 70
HZ12	Zhang R et al, 2018	10 Feb -19 Mar 2015	Beijing	30-65%	2.2-19	19-61	16-30
HZ13	Ma et al, 2018	25 Nov-3 Dec 2015	Beijing	_	up to ~20	up to ~150	up to ~65
HZ14	Guo et al, 2019	21 Dec. 2015 - 1 Jan 2016	Nanjing	~65-95%	12	46	25
HZ15	Zhang Y.T. et al, 2018	Select days in 2015	Ji'nan, Shandong	76-91%	5-30	_	20-110
HZ16	Zhang C.Y. et al, 2018	Nov 2015-Mar 2016	Handan, Hebei	~10-88%	36-77	28-55	up to 120
HZ17	Li et al, 2019	1-9 Dec 2016 19-24 Dec 2016	Yangtze River Delta	~60-85%	8.2 9.3	41 43	13.6 11.5
HZ18	Chi et al, 2018	Nov. 2016-Jan 2017	Beijing	75-100%	7.6	56	16.3
HZ19	Wang et al., 2019	8-25 Jan 2018	Zhengzhou	71% (~30-98%)	8-23	21-63	39

* The studies are in the order of observation time.
^ The references in this table correspond to references 37-55 in the reference list.
# SO_2 and NO_x data were converted to ppb at 20°C and 1 atm if they were presented in the unit of $\mu g\ m^{-3}$ in the paper. When data were not available in numerical forms, they were read from figures.
ϕ Unable to infer numerical data from the paper.

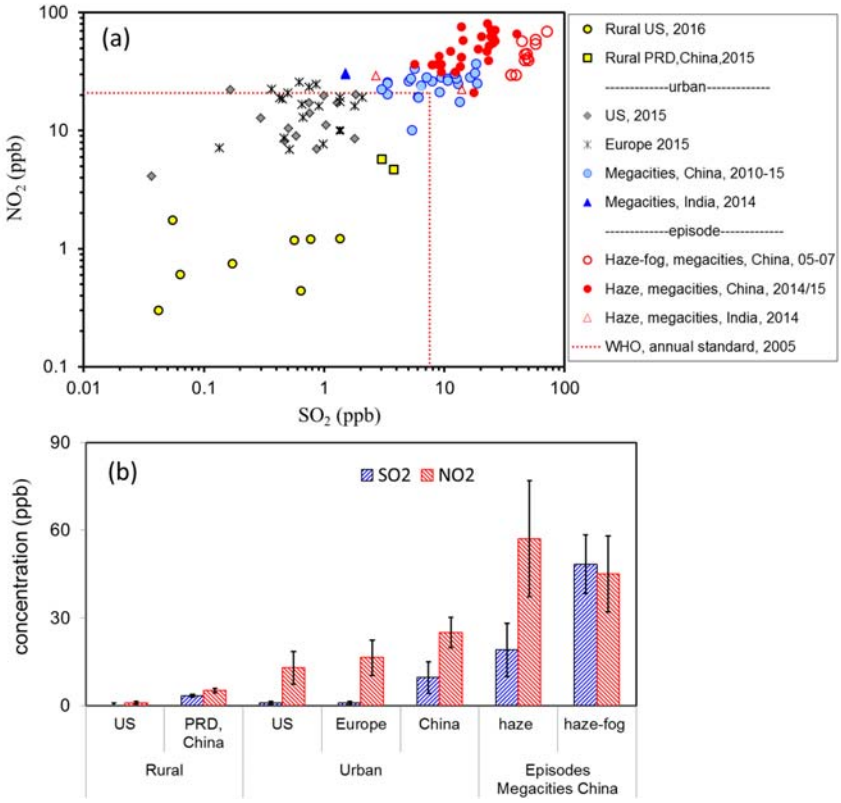

Figure S1 | Worldwide pairs of SO_2 and NO_2 concentrations. (a) Scatter plots of the SO_2 and NO_2 concentration in each scenario. The same figure is plotted on a linear scale in Figure 1 of the main text. (**b)** Average concentrations of SO_2 and NO_2 observed in each scenario. Error bars represent the standard deviation of the data set.

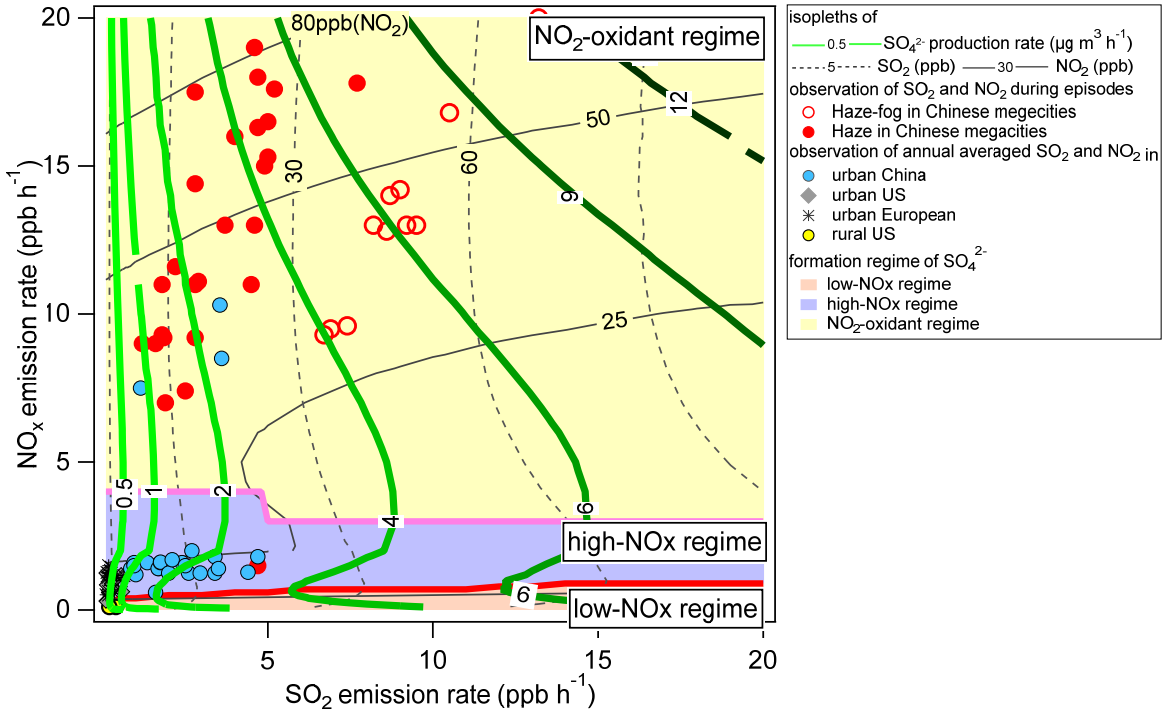

Figure S2 | SO_4^{2-} formation potential as a function of NO_x and SO_2 emission rates. The same figure is plotted on a logarithm scale in Figure 2 of the main text. The colored curves show isopleths of the SO_4^{2-} production rates. Numbers on the curves are the SO_4^{2-} production rates in μg m^{-3} h^{-1}. The solid and dashed curves and the numbers on them show isopleths of the daily averaged NO_2 and SO_2 concentration, respectively. The markers represent the NO_2 and SO_2 levels observed around the world (as those shown in Figure 1). The solid red and pink lines separate three individual SO_4^{2-} formation regimes.

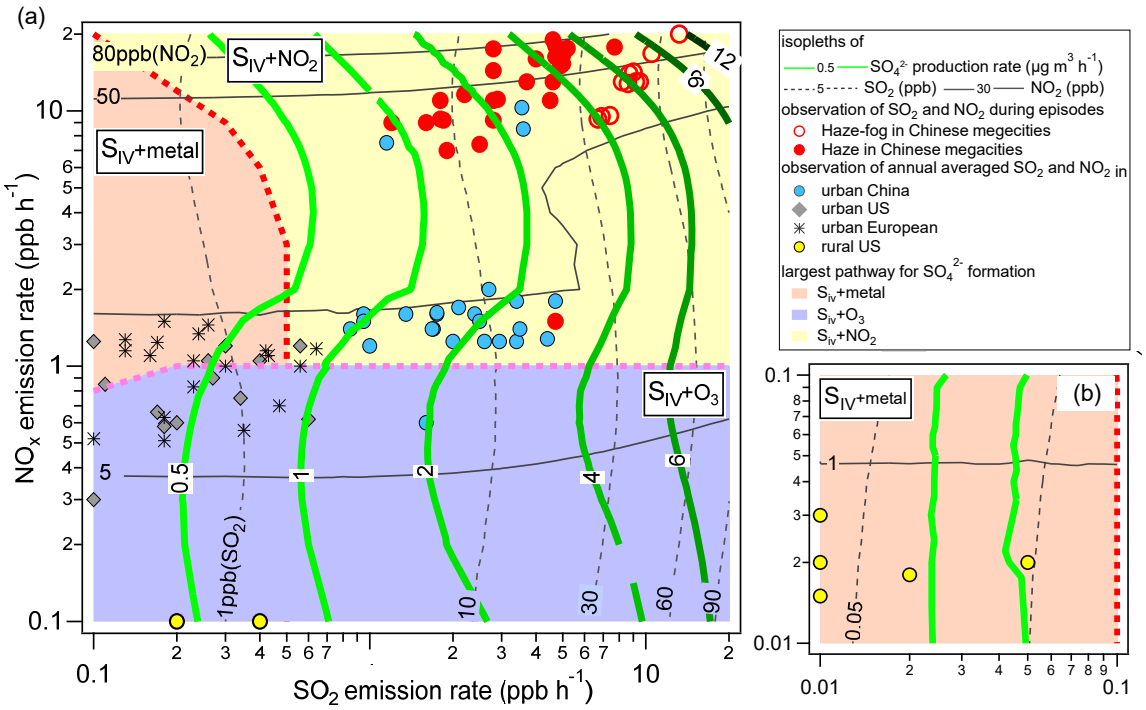

Figure S3 | Most important SO_4^{2-} production pathway at different NO_x and SO_2 emission levels under haze-fog conditions. (a) SO_4^{2-} production rates under NO_x and SO_2 emission levels ranging from 0.1-20 ppb h^{-1}. (b) SO_4^{2-} production rates under low NO_x and SO_2 emission levels are shown. This figure reproduces Figure 2 in the main text, with the difference being that regimes are now demarcated by the dominant SO_2 oxidation pathway. The simulation was conducted at an aqueous phase pH of 5.6. The colored curves show isopleths of the SO_4^{2-} production rates, with the colder colors representing lower rates and warmer colors representing higher rates. Numbers on the curves (e.g., 0.5, 1, 2, etc.) are the SO_4^{2-} production rates in μg m^{-3} h^{-1}. The solid curves and the numbers on them show isopleths of the daily averaged NO_2 concentration (e.g., 5, 25, etc.). The dashed curves and the numbers on them indicate isopleths of the daily average SO_2 concentration (e.g., 1, 10 and etc.). The markers represent the NO_2 and SO_2 levels observed around the world (as those shown in Figure 1a). The dashed red and pink lines separate the reaction pathway regimes. The smaller plot in the right-bottom exhibits the most important SO_4^{2-} pathways under lower NO_2 and SO_2 emission levels.

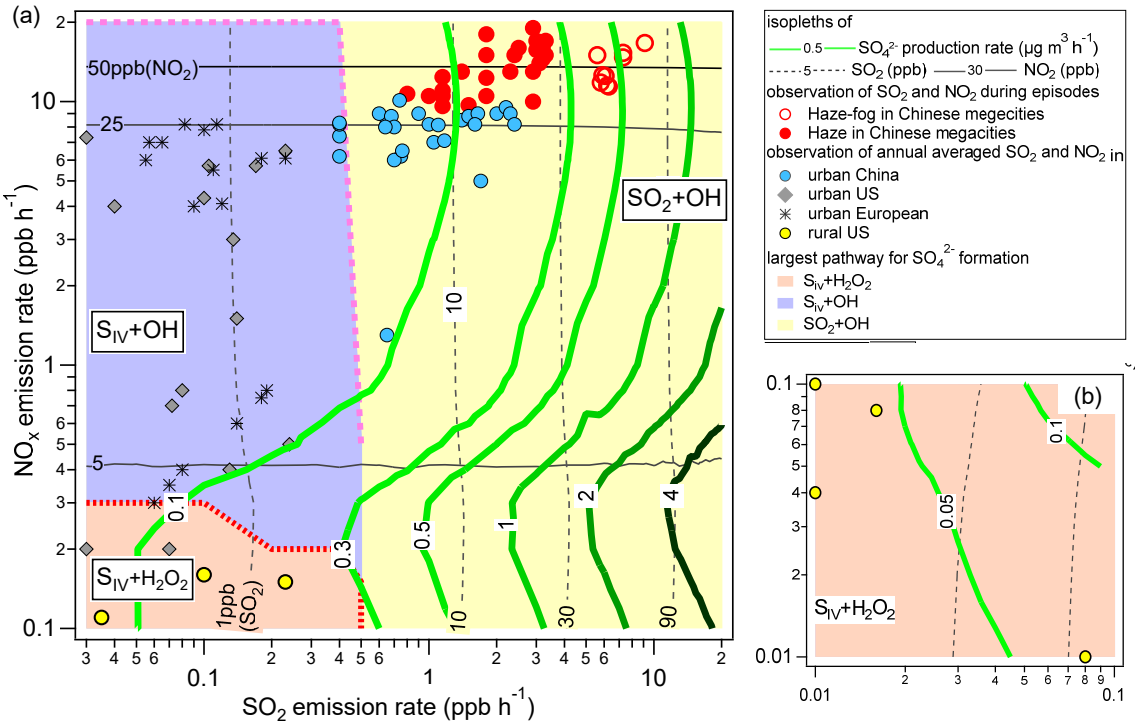

Figure S4 | Important pathway accounting for SO_4^{2-} production at different NO_x and SO_2 emission levels under clean fog conditions. (a) SO_4^{2-} production rates under NO_x and SO_2 emission levels ranging from 0.1-20 ppb h^{-1}. (b) SO_4^{2-} production rates under low NO_x and SO_2 emission levels are shown. This figure reproduces Figure 3 in the main text, with the difference being that regimes are now demarcated by the dominant SO_2 oxidation pathway. The simulation was conducted at an aqueous phase *p*H of 4.7. The colored curves show isopleths of the SO_4^{2-} production rates, with the colder colors representing lower rates and warmer colors representing higher rates. Numbers on the curves (e.g., 0.5, 1, 2, etc.) are the SO_4^{2-} production rates in μg m^{-3} h^{-1}. The solid curves and the numbers on them show isopleths of the daily averaged NO_2 concentration (e.g., 5, 25, etc.). The dashed curves and the numbers on them indicate isopleths of the daily average SO_2 concentration (e.g., 1, 10 and etc.). The markers represent the NO_2 and SO_2 levels observed around the world (as those shown in Figure 1a). The dashed red and pink lines separate the reaction pathway regimes. The smaller plot on the right-bottom exhibits the most important SO_4^{2-} pathways under lower NO_2 and SO_2 emission levels. In the NO_2-oxidant regime (shown in Fig. 3), while the leading oxidant of $SO_2/S_{(IV)}$ is gas-phase OH contributing to 33-42% of sulfate formation, NO_2 (aq) is still a significant oxidant accounting for 7-18% of sulfate formation.

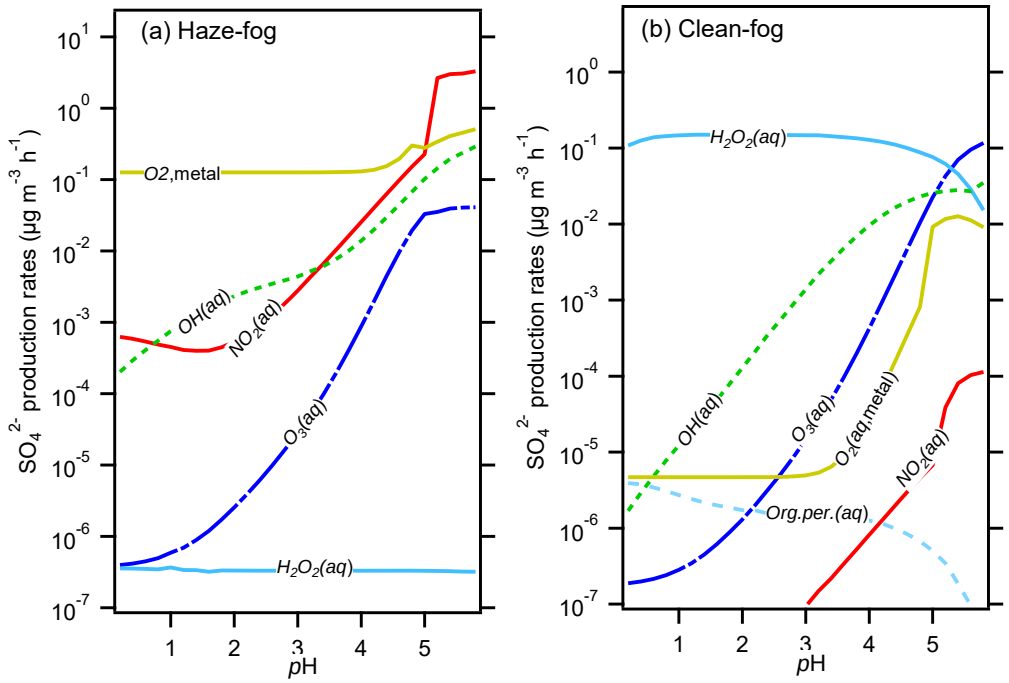

Figure S5 | Comparison of sulfate aqueous formation pathways as a function of aqueous phase pH. (a) typical haze-fog condition with NO_x and SO_2 emission rates of 9 and 8 ppb h^{-1}, respectively; (b) typical clean-fog condition with NO_x and SO_2 emission rates of 0.05 and 0.05 ppb h^{-1}.

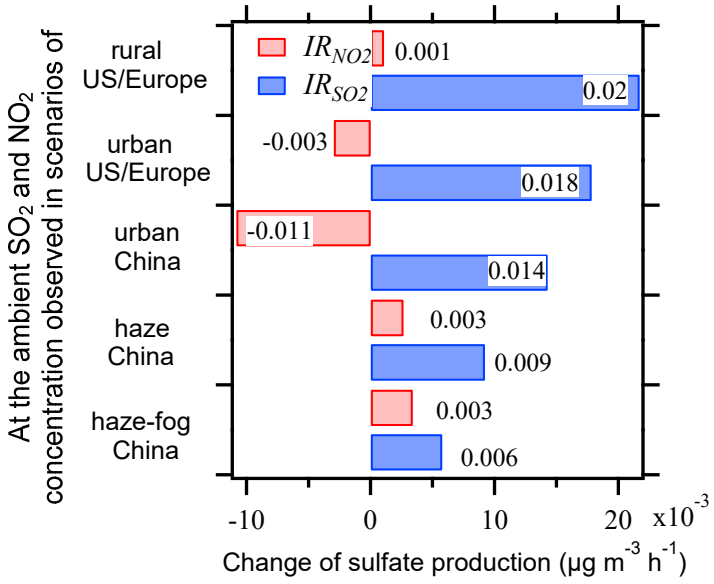

Figure S6 | Predicted reduction of SO_4^{2-} production rate (μg m^{-3} h^{-1}) in response to 0.01 ppb h^{-1} reduction of NO_x or SO_2 emissions. Simulation are conducted under atmospheric physical conditions of typical haze-fog events with an aqueous phase pH of 5.6. The sensitivity is shown for five scenarios of ambient SO_2 and NO_2 concentrations corresponding to those recorded at worldwide locations in Figure 1.

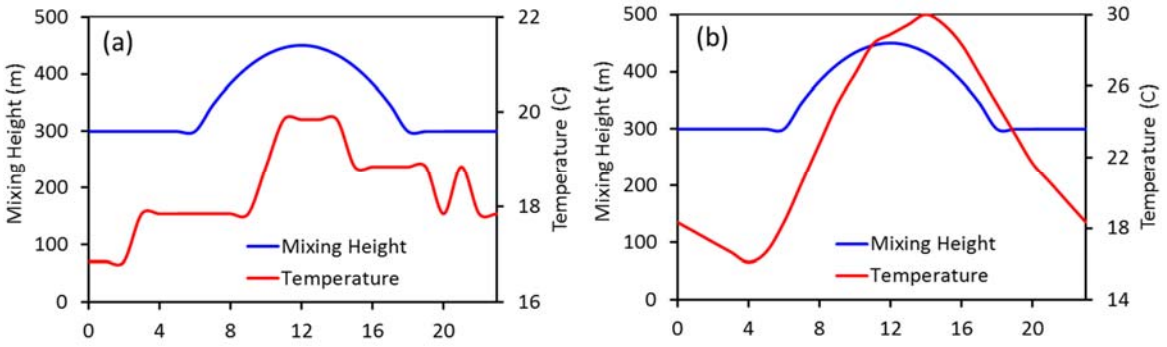

Figure S7 | The input of mixing height and temperature in the model for (a) the haze-fog episodes in winter Guangzhou, China, and (b) clean-fog in summer in central Pennsylvania, U.S.

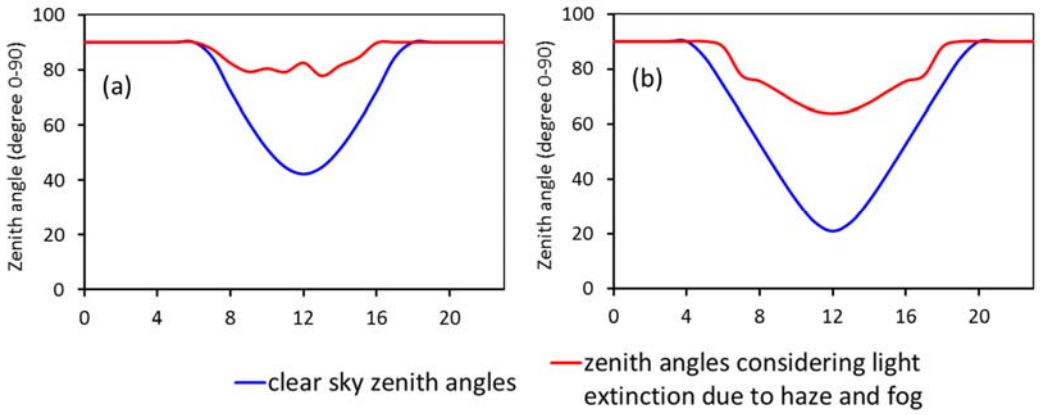

Figure S8 | 24-hour zenith angles in clear sky, and zenith angles accounting for light extinction that were used for the simulation of (a) the haze-fog episodes in winter Guangzhou, China, and (b) clean-fog in summer in central Pennsylvania, U.S.

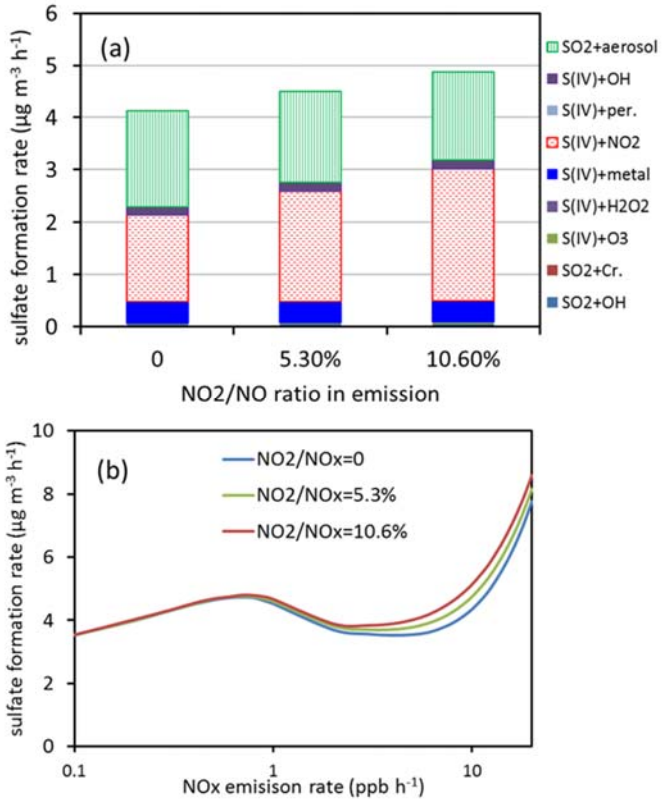

Figure S9 | Sensitivity of sulfate formation rate in response to different NO_2 fractions (%) in raw NO_x emissions during typical haze-fog episode. (a) Comparison of sulfate formation rates from individual oxidation pathways corresponding to three f(NO_2) assumptions, and (b) Comparison of overall sulfate formation rate as a function of NO_x emission rate corresponding to three f(NO_2) assumptions.

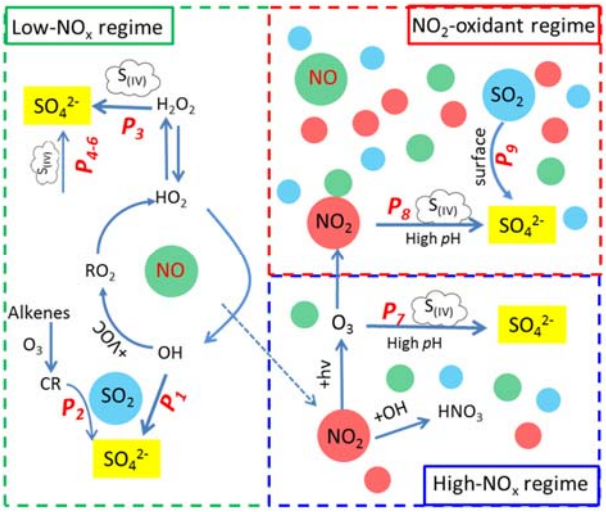

Seq.	Pathways to produce SO_4^{2-}
P_1	$SO_2 + OH \longrightarrow SO_4^{2-} + HO_2$
P_2	$SO_2 + CR \longrightarrow SO_4^{2-} + others$
P_3	$HSO_3^- + H_2O_2(aq) \longrightarrow SO_4^{2-} + H^+ + H_2O$
P_4	$S_{(IV)} + 1/2O_2(aq) \xrightarrow{Mn^{2+},Fe^{3+}} SO_4^{2-}$
P_5	$S_{(IV)} + OH(aq) \longrightarrow SO_4^{2-} + others$
P_6	$S_{(IV)} + organic\ peroxide(aq) \longrightarrow SO_4^{2-} + others$
P_7	$S_{(IV)} + O_3(aq) \longrightarrow SO_4^{2-} + O_2$
P_8	$S_{(IV)} + NO_2(aq) \longrightarrow SO_4^{2-} + HONO$
P_9	$SO_2 + Aerosol\ surface \longrightarrow SO_4^{2-}$

Figure S10 | Conceptual diagram showing major oxidation pathways contributing to SO_4^{2-} production in the three formation regimes. The *high-NO_x* and *NO_2-oxidant regimes* were constrained to a high aqueous phase *p*H condition which is frequently observed during haze-fog episodes in Chinese megacities.

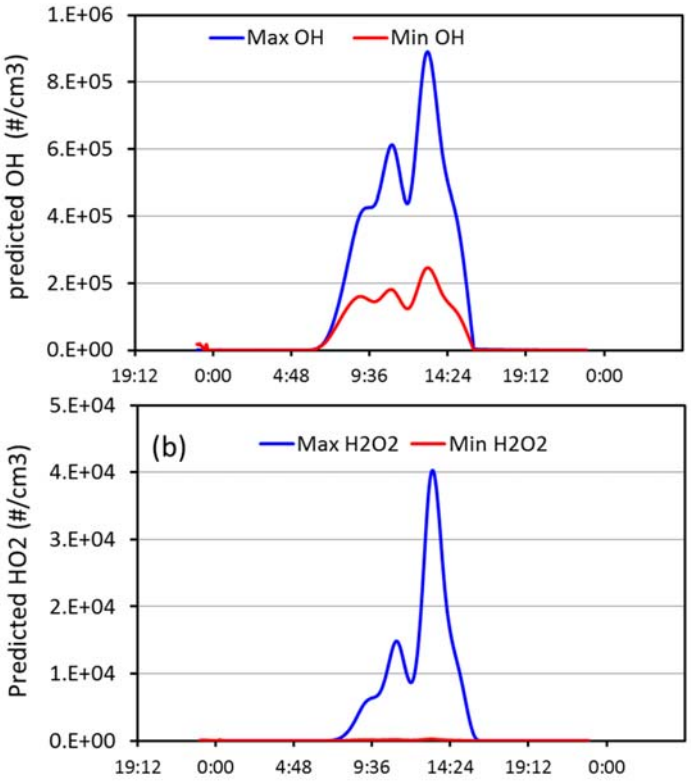

Figure S11 | Diurnal variation of OH and H_2O_2 predicted for the typical haze-fog episodes.

References:

1. Wennberg P. O. Let's abandon the "high NO_x" and "low NO_x" terminology. *IGACnews*. **50**, 3-4 (2013).
2. Sillman .S. The relation between ozone, NOx and hydrocarbons in urban and polluted rural environment. *Atmos. Environ.* **33**, 1821-1845 (1999).
3. Cheng, Y. F. et al. Reactive nitrogen chemistry in aerosol water as a source of sulfate during haze events in China. Sci. Adv. 2, e1601530 (2016).
4. Tan, Z. F. et al. Wintertime photochemistry in Beijing: Observations of ROx radical concentrations in the North China Plain during the BEST-ONE campaign, *Atmos. Chem. Phys.*, **18**, 12391–12411 (2018).
5. USEPA. Air quality data collected at outdoor monitors across the US. Available at: https://www.epa.gov/outdoor-air-quality-data
6. HKEPD. Pearl River Delta regional air quality monitoring report, Available at: https://www.epd.gov.hk/epd/english/resources_pub/publications/m_report.html
7. European environment agency, Sulphur Dioxide (SO_2): annual mean concentrations in Europe, available at http://www.eea.europa.eu/themes/air/interactive/so2
8. European environment agency, Nitrogen Dioxide (NO_2): annual mean concentrations in Europe, available at: http://www.eea.europa.eu/themes/air/interactive/no2
9. HKEPD, Pearl River Delta Regional Air Quality Monitoring Report for Year 2010. Available at: https://www.epd.gov.hk/epd/english/resources_pub/publications/m_report.html
10. BMEPB, Beijing environmental statement, 2010, in Chinese
11. SHEPB, Shanghai environmental statement, 2010, in Chinese
12. BMEPB, Beijing environmental statement, 2015, in Chinese
13. SHEPB, Shanghai environmental statement, 2015, in Chinese
14. JNEPB, Jinan environmental statement, 2015, in Chinese
15. NJEPB, Nanjing environmental statement, 2014, in Chinese
16. HZEPB, Hangzhou environmental statement, 2014, in Chinese
17. CDEPB, Chengdu environmental statement, 2014, in Chinese
18. Lu, C. S. et al. Chemical composition of fog water in Nanjing area of China and its related fog microphysics. *Atmos. Res*. 97, 47-69 (2010).
19. Wu D. et al. Study on the chemical characteristics of polluting fog in Guangzhou area in spring. *J. Trop. Meteorol*. 15, 68-72 (2009).
20. Xue J., Yuan Z. B., Lau A. K. H. & Yu J. Z., Insights into factors affecting nitrate in PM2.5 in a polluted high NOx environment through hourly observations and size distribution measurements, *J Geophys Res Atmos.* **119**, 4888-4902, doi: 10.1002/2013JD021108 (2014).
21. Hu et al., The variation of characteristics of individual particles during the haze evolution in the urban Shanghai atmosphere, *Atmos. Res.* **181**, 95-105 (2016).
22. Ma, X.& Jia, H., Particulate matter and gaseous pollutions in three megacities over China: Situation and implication, *Atmos. Environ.* **140**, 476-494, (2016)..
23. Zheng et al. Exploring the severe winter haze in Beijing: the impact of synoptic weather, regional transport and heterogeneous reaction, *Amos. Chem. Phys.* **15**, 2969-2983 (2015).
24. Tiwari, et al., Statistical evaluation of PM10 and distribution of PM1, PM2.5, and PM10 in ambient air due to extreme fireworks episodes (Deepawali festivals) in megacity Delhi, *Nat. Hazards*, **61**, 521-531, (2012).
25. WHO. Ambient (outdoor) air quality and health. Available at: http://www.who.int/news-room/fact-sheets/detail/ambient-(outdoor)-air-quality-and-health
26. Straub, D. J., Hutchings, J. W. & Herckes, P. Measurements of fog composition at a rural site. *Atmos. Environ.* **47,** 195-205 (2012).
27. Kleinman L. I. Seasonal dependence of boundary layer peroxide concentration: the low and high NOx regimes. *J. Geophys. Res.* **96,** 20721-20733 (1991).
28. Seinfeld, J. H., Pandis, S. N. Atmospheric Chemistry and Physics. *Wiley Express* (2006).

29. Martin, L. R. & Good, T. W. Catalyzed oxidation of sulfur-dioxide in solution - the Iron-Manganese Synergism. *Atmos. Environ.* **25,** 2395-2399 (1991).

30. Martin, L. R., & Hill, M. W. The effect of ionic strength on the manganese catalyzed oxidation of sulfur(IV), *Atmos. Environ.* **21**, 2267-2270 (1987).

31. Lee, Y. N.; Schwartz, S. E., Kinetics of oxidation of aqueous sulfur(IV) by nitrogen dioxide. In Precipitation Scavenging, Dry Deposition and Resuspension, H.R. Pruppacher, R. G. Semonin, and W. G. N. Slinn, eds., Elsevier, New York (1983).

32. Xue, J. *et al*. Sulfate formation enhanced by a cocktail of high NOx, SO_2, particulate matter, and droplet pH during haze-fog events in megacities in China: an observation-based modeling investigation. *Environ. Sci. Technol*. **50**, 7325-7334 (2016).

33. Li, P. F. *et al.* Fog water chemistry in Shanghai. *Atmos. Environ.* **45,** 4034-4041 (2011).

34. Straub, D. J., Hutchings, J. W. & Herckes, P. Measurements of fog composition at a rural site. *Atmos. Environ.* **47**, 195-205 (2012).

35. Heikes, B. G. et al. Hydrogen peroxide and methylhydroperoxide distributions related to ozone and odd hydrogen over the North Pacific in the fall of 1991. *J. Geophys. Res*, **101**, (D1), 1891-1905 (1996).

36. Raja, S. et al. Fog chemistry in the Texas-Louisiana Gulf Coast corridor. *Atmos. Environ.* **42**, (9), 2048-2061 (2008).

37. Han, T. T. et al. Role of secondary aerosols in haze formation in summer in the Megacity Beijing. *J. Environ. Sci.* **31**, 51-60 (2015).

38. Kong, L. D. et al. Trends in heterogeneous aqueous reaction in continuous haze episodes in suburban Shanghai: An in-depth case study. *Sci. Tot. Environ.* **634**, 1192-1204 (2018).

39. Xie, Y. N. et al. Enhanced sulfate formation by nitrogen dioxide: Implications from in situ observations at the SORPES station. *J. Geophy. Res. Atmosphere* **120**, 12679-12694 (2015).

40. Zhao, M. F., Xiu, G. L., Qiao, T. & Yu, J. Z. Characteristics of haze pollution episodes and analysis of a typical winter haze process in Shanghai. *Aerosol & Air Qual. Res.***16**, 1625-1637 (2016).

41. He, H. et al. Mineral dust and NOx promote the conversion of SO2 to sulfate in heavy pollution days. *Sci. Rep.*, **4**, 4172 (2014).

42. Huang, L. et al, Enhanced sulfate formation through SO_2+NO_2 heterogeneous reactions during heavy winter haze in the Yangtze River Delta region, China. *Atmos. Chem. Phys. Discuss.* (2019) https://doi.org/10.5194/acp-2019-292.

43. Wang, H. L. et al, Regional Characteristics of Air Pollutants during Heavy Haze Events in the Yangtze River Delta, China. *Aerosol & Air Qual. Res.***16**, 2159-2171 (2016).

44. Gao, M. et al, Improving simulations of sulfate aerosols during winter haze over Northern China: the impacts of heterogeneous oxidation by NO_2. *Front. Environ. Sci. Eng*., **10(5)**, 16 (2016).

45. Liu, P.F. et al., The possible contribution of the periodic emissions from farmers' activities in the North China Plain to atmospheric water-soluble ions in Beijing. *Atmos. Chem. Phys*., **16**, 10097–10109 (2016).

46. He, P.Z. et al., Isotopic constraints on heterogeneous sulfate production in Beijing haze. *Atmos. Chem. Phys*. **18**, 5515–5528 (2018).

47. Chen, D., Liu, Z.Q., Fast, J. & Ban, J. M. Simulations of sulfate–nitrate–ammonium (SNA) aerosols during the extreme haze events over northern China in October 2014. *Atmos. Chem. Phys*. **16**, 10707–10724 (2016).

48. Zhang, R., et al, Secondary inorganic aerosols formation during haze episodes at an urban site in Beijing, China. *Atmos. Environ.***177**, 275-282 (2018).

49. Ma, J. Z. et al, NO_x promotion of SO_2 conversion to sulfate: An important mechanism for the occurrence of heavy haze during winter in Beijing. *Environ. Poll.* **233**, 662-229 (2018).

50. Guo, Z.Y. et al, Study on pollution behavior and sulfate formation during the typical haze event in Nanjing with water soluble inorganic ions and sulfur isotopes. *Atmos. Res.* **217**, 198-207 (2019).

51. Zhang, Y. T. et al, Trend in fine sulfate concentrations and the associated secondary formation processes at an urban site in North China. *Aerosol & Air Qual. Res.***18**, 1519-1530 (2018).

52. Zhang, C.Y. et al, Evolution of key chemical components in $PM_{2.5}$ and potential formation mechanisms of serious haze events in Handan, China. *Aerosol Air Qual. Res.***18**, 1545-1557 (2018).

53. Li, M.M. et al, Formation and evolution mechanisms for two extreme haze episodes in the Yangtze River Delta Region of China during winter 2016. *J. Geophy. Res. Atmosphere* **124**, 3607-3623 (2019).

54. Chi, X.Y. et al, Acidity of aerosols during winter heavy haze events in Beijing and Gucheng, China. *J. Meteor. Res.*, **32**(1), 14–25 (2018).

55. Wang, S.B. et al, Insight into the formation of secondary inorganic aerosol based on high-time-resolution data during haze episodes and snowfall periods in Zhengzhou, China. *Sci. Tot. Environ*. **660**, 47-56 (2019).